BBA - Bioenergetics 1862 (2021) 148330

Contents lists available at ScienceDirect

BBA - Bioenergetics

journal homepage: www.elsevier.com/locate/bbabio

Gas channel rerouting in a primordial enzyme: Structural insights of the carbon-monoxide dehydrogenase/acetyl-CoA synthase complex from the acetogen *Clostridium autoethanogenum*

Olivier N. Lemaire, Tristan Wagner *

Max Planck Institute for Marine Microbiology, Celsiusstraße 1, 28359 Bremen, Germany

ARTICLE INFO

Keywords:
C_1-metabolism
Acetogenesis
CO-dehydrogenase/acetyl-CoA synthase
X-ray crystal structure
Gas channeling
Waste-gas conversion

ABSTRACT

Clostridium autoethanogenum, the bacterial model for biological conversion of waste gases into biofuels, grows under extreme carbon-monoxide (CO) concentrations. The strictly anaerobic bacterium derives its entire cellular energy and carbon from this poisonous gas, therefore requiring efficient molecular machineries for CO-conversion. Here, we structurally and biochemically characterized the key enzyme of the CO-converting metabolism: the CO-dehydrogenase/Acetyl-CoA synthase (CODH/ACS). We obtained crystal structures of natively isolated complexes from fructose-grown and CO-grown *C. autoethanogenum* cultures. Both contain the same isoforms and if the overall structure adopts the classic $\alpha_2\beta_2$ architecture, comparable to the model enzyme from *Moorella thermoacetica*, the ACS binds a different position on the CODH core. The structural characterization of a proteolyzed complex and the conservation of the binding interface in close homologs rejected the possibility of a crystallization artefact. Therefore, the internal CO-channeling system, critical to transfer CO generated at the C-cluster to the ACS active site, drastically differs in the complex from *C. autoethanogenum*. The 1.9-Å structure of the CODH alone provides an accurate picture of the new CO-routes, leading to the ACS core and reaching the surface. Increased gas accessibility would allow the simultaneous CO-oxidation and acetyl-CoA production. Biochemical experiments showed higher flexibility of the ACS subunit from *C. autoethanogenum* compared to *M. thermoacetica*, albeit monitoring similar CO-oxidation and formation rates. These results show a reshuffling of internal CO-tunnels during evolution of these *Firmicutes*, putatively leading to a bidirectional complex that ensure a high flux of CO-conversion toward energy conservation, acting as the main cellular powerplant.

1. Introduction

Carbon monoxide (CO) is a poisonous and chemically reactive gas. However, some microorganisms tolerate CO and even use its high reducing power for metabolic needs [1,2]. One of these specialists is the bacterium *Clostridium autoethanogenum*. Isolated through its ability to grow on CO as sole carbon and energy source, this genetically tractable model organism is a biotechnological chassis: it is used in bioremediation to turn waste gases (*e.g.* from steel mill industries), rich in CO, into valuable compounds such as acetate, ethanol and 2, 3-butanediol [3–7]. In large-scale bioreactors the main substrate for the bacterium is industrial syngas, containing up to 50% of CO at 200 kPa. Under such extreme conditions *C. autoethanogenum* still exhibits a robust growth, with its whole metabolism being fully adapted to CO-based autotrophy [3–5,7–9]. This acetogenic bacterium uses the Wood-Ljungdahl pathway for carbon fixation and energy conservation, a primordial metabolism responsible for up to 20% of the global CO_2-fixation [10,11]. The Wood-Ljungdahl pathway consists of two branches, the "methyl" and "carbonyl" branches, which unite to ultimately generate acetyl-coenzyme A (acetyl-CoA), one of the elementary brick of every cell component (Fig. 1) [10–14]. In acetogens, the methyl-branch starts by a CO_2 reduction into formate, which is further condensed on the C_1-carrier tetrahydrofolate, at the expense of one molecule of ATP. The formyl-tetrahydrofolate is further dehydrated to methenyl-tetrahydrofolate, followed by two reduction reactions, which result into methyl-tetrahydrofolate. In the carbonyl-branch, CO_2 is reduced into CO

Abbreviations: CO, carbon monoxide; CO_2, carbon dioxide; CODH, CO-dehydrogenase; CoA, coenzyme A; ACS, acetyl-CoA synthase; SDS/hrCN PAGE, sodium dodecylsulfate/high resolution clear native polyacrylamide gel electrophoresis; MV, methyl-viologen.

* Corresponding author.
E-mail address: twagner@mpi-bremen.de (T. Wagner).

https://doi.org/10.1016/j.bbabio.2020.148330
Received 4 May 2020; Received in revised form 1 October 2020; Accepted 15 October 2020
Available online 17 October 2020

which is further used to synthetize acetyl-CoA by combining the CoA-SH and the methyl group from the methyl-branch. The methyl-group is carried by an intermediate cobalamin-containing Fe—S protein [14,15].

Based on the thermodynamics of the Wood-Ljungdahl pathway, CO-conversion provides more cellular energy (theoretically, 2–3 mol of ATP per acetate formed) than H_2 and CO_2 utilization (theoretically, 1–2 mol of ATP per acetate formed through CO_2-fixation) [16,17]. However, the high reactivity of CO prevents the survival of most microorganisms at the CO-concentrations required for an optimal growth.

The fact that *C. autoethanogenum* can thrive in high CO-levels indicates an adaptation of the enzymes of the Wood-Ljungdahl pathway to higher CO-tolerance (resulting in *e.g.* the seven-subunits CO_2-reducing Hyt/Fdh complex [3,14]). At the same time the CO-conversion systems must be on first line with a robust activity to reduce the amount of cellular CO. The key enzyme of the CO-conversion process, the CO-dehydrogenase (CODH), is considered as the prime CO sink. Under growth based on H_2 and CO_2, the CODH orchestrates the first step of the carbonyl-pathway, allowing CO generation by using electrons from low potential ferredoxins (Fig. 1). The reverse reaction occurs during CO-dependent autotrophic growth and provides the reducing equivalents for the acetogen to feed the Wood-Ljungdahl pathway to fix carbon and provide cellular energy [3,5,7,10,14,18]. The genome of *C. autoethanogenum* encodes three isoforms of the CODH but only one, encoded by the CAETHG_1620–1621 locus, is necessary for autotrophic growth under H_2 plus CO_2 or CO [5,7,19]. This CODH gene is located in a genomic cluster also containing the sequence coding for the acetyl-CoA synthase (ACS), the enzyme responsible of the combination of CO, methyl- and HS-CoA to form acetyl-CoA (Fig. 1). The latter is mainly used to generate ATP from acetate, ethanol and 2, 3-butanediol release and only a small fraction is being kept for carbon-assimilation [9,20]. CODH and ACS are known to form a physiological complex and the intensive work on the prototypical $\alpha_2\beta_2$ CODH/ACS complex from the acetogenic model *Moorella thermoacetica* (*Mt*CODH/ACS) unraveled its mechanism. The whole process occurs in three steps: (i) by using electrons obtained from ferredoxin oxidation, CO_2 is reduced to CO at the C-cluster in the CODH active site; (ii) CO is internally guided to the active site of the acetyl-CoA synthase, harboring the A-cluster; (iii) CO is combined to HS-CoA and a methyl group, obtained from the methyl-branch of the Wood-Ljungdahl pathway, to generate acetyl-CoA [21] (Fig. 1). The internal CO-channel, identified from biochemistry experiments and visualized by Xenon pressurizing crystallographic structures [22,23], prevents a toxic and energy-losing CO leakage.

Under autotrophic CO-growth of *C. autoethanogenum*, only one CODH can be detected, belonging to a CODH/ACS complex (*Ca*CODH/ACS) [5]. In comparison, under similar growth conditions the CO-oxidizer *Carboxydothermus hydrogenoformans* (abbreviated as *Ca. hydrogenoformans* to differentiate the genera *Clostridium* and *Carboxydothermus*) uses at least two monofunctional CODH: one dedicated for acetyl-CoA synthesis and the second one for energy-conserving CO-oxidation [24]. With only one enzyme, the CO-metabolism of *C. autoethanogenum* becomes puzzling. How could the CODH, when connected to the ACS, consume CO at high turnover if the C-cluster is concealed within the enzyme? Should a CO_2-reduction to CO precede the acetyl-CoA synthesis or can CO directly access the ACS A-cluster? Here, we answer these questions by isolating the native *Ca*CODH/ACS complex and presenting the molecular details of its assembly. Surprisingly, our results indicate that CODH from *M. thermoacetica* and *C. autoethanogenum* bind the ACS in a completely different fashion. As a consequence, the internal gas channel is reorganized, leading to the usage of new and unsealed channels. We hypothesize that the reshuffling and sur-numerous tunnels make the enzyme from *C. autoethanogenum* a modular one, suitable for all CO concentrations.

2. Materials and methods

2.1. Bacterial strains and growth conditions

C. autoethanogenum DSM 10061 and *M. thermoacetica* DSM 521 were

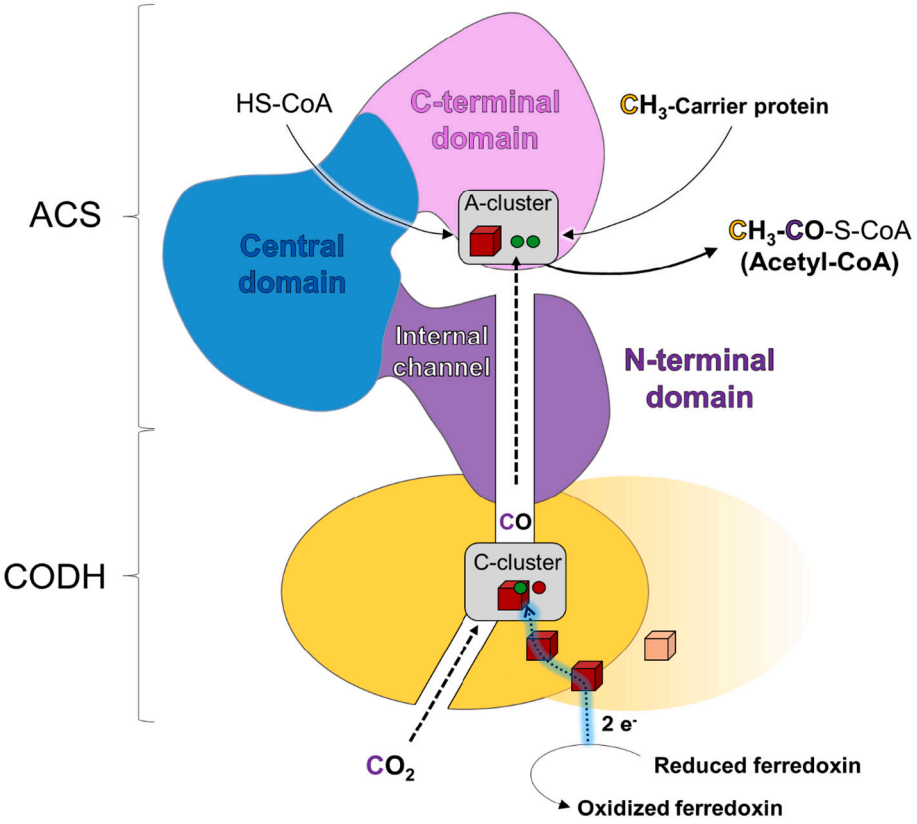

Fig. 1. Scheme of the canonical mechanism of the CODH/ACS complex. The bacterial CODH/ACS complex organizes as a $\alpha_2\beta_2$, the CODH forming the dimeric interface. Using low potential electrons obtained by ferredoxin oxidation (electron transfer is shown as a dark blue arrow), CO_2 is reduced to CO at the Fe-[$NiFe_3S_4$] active site of the CODH: the C-cluster. CO is channeled in the complex to reach the catabolic A-cluster, harbored in the C-terminal domain of the ACS. The A-cluster combines the CO with a methyl group which is carried by the corrinoid FeS protein carrier and HS-CoA to ultimately form acetyl-CoA. Green and red spots symbolize Ni and Fe atoms, respectively. Red cubes represent cubane [Fe_4S_4], an Fe atom is replaced by Ni in the C-cluster.

obtained from the Deutsche Sammlung von Mikroorganismen und Zellkulturen GmbH, Braunschweig, Germany. *C. autoethanogenum* was cultivated under strict anaerobic conditions at 37 °C in CaGM growth medium [5] in which titanium citrate was omitted. For heterotrophic growth, 10 g/L of fructose was added to the medium, the gas phase initially contained 100 kPa of a H_2/CO_2 mixture (80:20%). For autotrophic CO-growth, no fructose was added to the medium and the gas phase contained 100 kPa of 100% CO. *M. thermoacetica* was cultivated under strict anaerobic conditions at 55 °C in CaGM medium supplemented with anoxic and 40 mM of sterile potassium phosphate buffer pH 6.0, 100 mM NaCl and 5 g/L of yeast extract. Cell growth was monitored spectrophotometrically by measuring the optical density at 600 nm (OD_{600}) and changes in headspace pressure. The cells were harvested in late-exponential phase by centrifugation and kept frozen at −80 °C in anaerobic conditions, unless stated otherwise.

2.2. Protein purification

Cell lysis and preparation of extracts were performed in an anaerobic chamber filled with a N_2/CO_2 atmosphere (90:10%) at room temperature. The cells were lysed *via* sonication followed by three rounds of French Press at around 1000 PSI (6.895 MPa). To guarantee a minimum oxygen contamination, the French press cell was prior flushed with N_2 and washed twice with anoxic buffer. Crude extracts were prepared by removing the cell debris and unbroken cells *via* centrifugation at 16,250 *g* for 30 min at room temperature. Soluble extracts were prepared by ultracentrifugation at 140,000 *g* for 1 h at 4 °C. Protein purification was carried out under anaerobic conditions in a Coy tent with a N_2/H_2 atmosphere (95:5%) at 20 °C. Samples were passed through 0.2 μm filters prior to loading on chromatography columns. The detailed native purification protocols for all enzymes are described in the Supplementary information.

During purification, multi-wavelength absorbance monitoring (at 280, 415 and 550 nm), sodium dodecylsulfate polyacrylamide gel electrophoresis (SDS-PAGE) and CODH activity measurement with methyl-viologen (MV) were used to follow the enzymes.

2.3. Limited proteolysis

Limited proteolysis experiments were carried out using trypsin from porcine pancreas (Carl Roth). Trypsin was activated for at least 1 h in anoxic 50 mM Tris-HCl buffer, pH 7.6; 10 mM $CaCl_2$ (Proteolysis Buffer) at 20 °C in an anaerobic Coy tent containing a N_2/H_2 atmosphere (95:5%).

For time lapse experiments, anaerobically purified and frozen stored *Ca*CODH/ACS and *Mt*CODH/ACS were diluted with the same buffer to a protein concentration of 1 g/L. Activated trypsin was added at a final concentration of 0.002 g/L (500:1 w/w ratio) and proteolysis was performed at 20 °C. At different time intervals, 4 μL of the proteolytic reaction was sampled and quenched by adding an equal volume of standard SDS Loading Buffer. Results were analyzed *via* SDS-PAGE.

For proteolytic fragments purification a similar protocol was used, except that the reaction was not quenched and that the reaction mixture was incubated for 30 min followed by the immediate loading on a Mono Q™ 5/50 GL (GE Healthcare, see supplementary protocol).

2.4. Crystallization

Crystallization was exclusively performed in an anoxic chamber (N_2/H_2, 95:5%) with anaerobic solutions. Crystals were obtained using the sitting drop method on a 96-well MRC 2 Crystallization Plates in polystyrene (SWISSCI) by initial screening at 20 °C. The crystallization reservoir contained 90 μL of mother liquor, the crystallization drop was formed of a mixture of 0.6 μL protein and 0.6 μL precipitant. Best diffracting crystals were obtained in the same conditions.

The best diffracting crystal of *Ca*CODH/ACS from heterotrophic growth on fructose was obtained by initial screening using the Wizard 3 & 4 screen from Jena Bioscience. The crystallization reservoir contained 100 mM BIS-TRIS propane, pH 6.5; 200 mM sodium fluoride and 20% (w/v) polyethylene glycol 3350. The initial protein concentration was 16.4 mg/mL. The best diffracting crystal of *Ca*CODH/ACS from autotrophic growth on CO was obtained using the same solution and the initial protein concentration was 15.2 mg/mL.

The best diffracting crystal of $CODH/ACS_N$ was obtained by initial screening using the Shotgun (SG1) screen from Molecular dimensions. The crystallization reservoir contained 200 mM magnesium chloride hexahydrate; 20% (w/v) polyethylene glycol 3350. The protein concentration was 28.5 mg/mL.

The best diffracting crystal of the CODH was obtained by initial screening using the Shotgun (SG1) screen from Molecular dimensions. The crystallization reservoir contained 200 mM magnesium acetate tetrahydrate; 20% (w/v) polyethylene glycol 3350. The protein concentration was 16.9 mg/mL.

2.5. Data collection and structural analysis

All crystals were fished, cryoprotected and flash frozen in liquid nitrogen under an anaerobic atmosphere (N_2/H_2, 95:5%). Crystals of *Ca*CODH/ACS obtained from fructose-grown or CO-grown conditions were flash-frozen after being soaked for 3–5 s in the crystallization solution supplemented with 20% v/v glycerol. $CODH/ACS_N$ crystals were soaked for 3–5 s in the crystallization solution supplemented with 25% v/v ethylene glycol prior to liquid nitrogen storage. CODH crystals were soaked for 3–5 s in the crystallization solution supplemented with 25% v/v glycerol prior to the transfer into liquid nitrogen.

The diffraction experiments were performed at 100 K on the beamline P13 from DESY (EMBL), Proxima 1 from SOLEIL and PXIII (X06DA) from SLS. The data were processed with XDS [25]. For the *Ca*CODH/ACS obtained from the CO-grown culture, the integrated data were scaled with SCALA from the CCP4 suite [26]. The three other datasets were anisotropic and therefore processed through the Staraniso server (http://staraniso.globalphasing.org/cgi-bin/staraniso.cgi) [27]. The first structure of the *Ca*CODH/ACS was solved by performing a single-anomalous dispersion experiment at the Fe K-edge. The substructure was elucidated by SHELX D [28]. By applying a resolution cut-off of 4.7 Å and a search for 7 anomalous scatterers, a CCall of 45.99% and a CCweak of 23.24% were obtained. Phasing, density modification and automatic building was performed by Autosol from the Phenix package [29]. The density modification has a map skew of 0.1 and a correlation of local root mean square density of 0.84. The three other structures were solved by molecular replacement, using the *Ca*CODH/ACS model as a template. All models were manually built *via* COOT [30] and refined with BUSTER (version 2.10.3) [31] or Phenix (version 1.17.1-3660) [29]. The *Ca*CODH/ACS complex derived from a CO-grown culture at low resolution was only refined with the low-resolution refinement software from the CCP4 package from the *Ca*CODH/ACS model of fructose-grown cells. The last refinement steps were performed with hydrogens in riding position for the CODH alone and the hydrogens were omitted in the final deposited model. The final models were all validated *via* the MolProbity server (http://molprobity.biochem.duke.edu) [32]. Data collection, refinement statistics and PDB code for the deposited models are listed in the Supplementary table. The figures were generated and rendered with PyMOL (Version 1.5, Schrödinger, LLC). Interface analysis was performed by the PDBePISA server (http://www.ebi.ac.uk/pdbe/prot_int/pistart.html) [33] using the PDB 6YTT *Ca*CODH/ACS structure (chain A and B) and PDB 1MJG *Mt*CODH/ACS (chain A and B on N). Internal tunnel prediction was performed by the CAVER tool [34] by applying a probe radius of 1.2 Å.

2.6. High resolution Clear Native PAGE (hrCN PAGE)

The hrCN PAGE protocol was adapted from Lemaire et al. (2018)

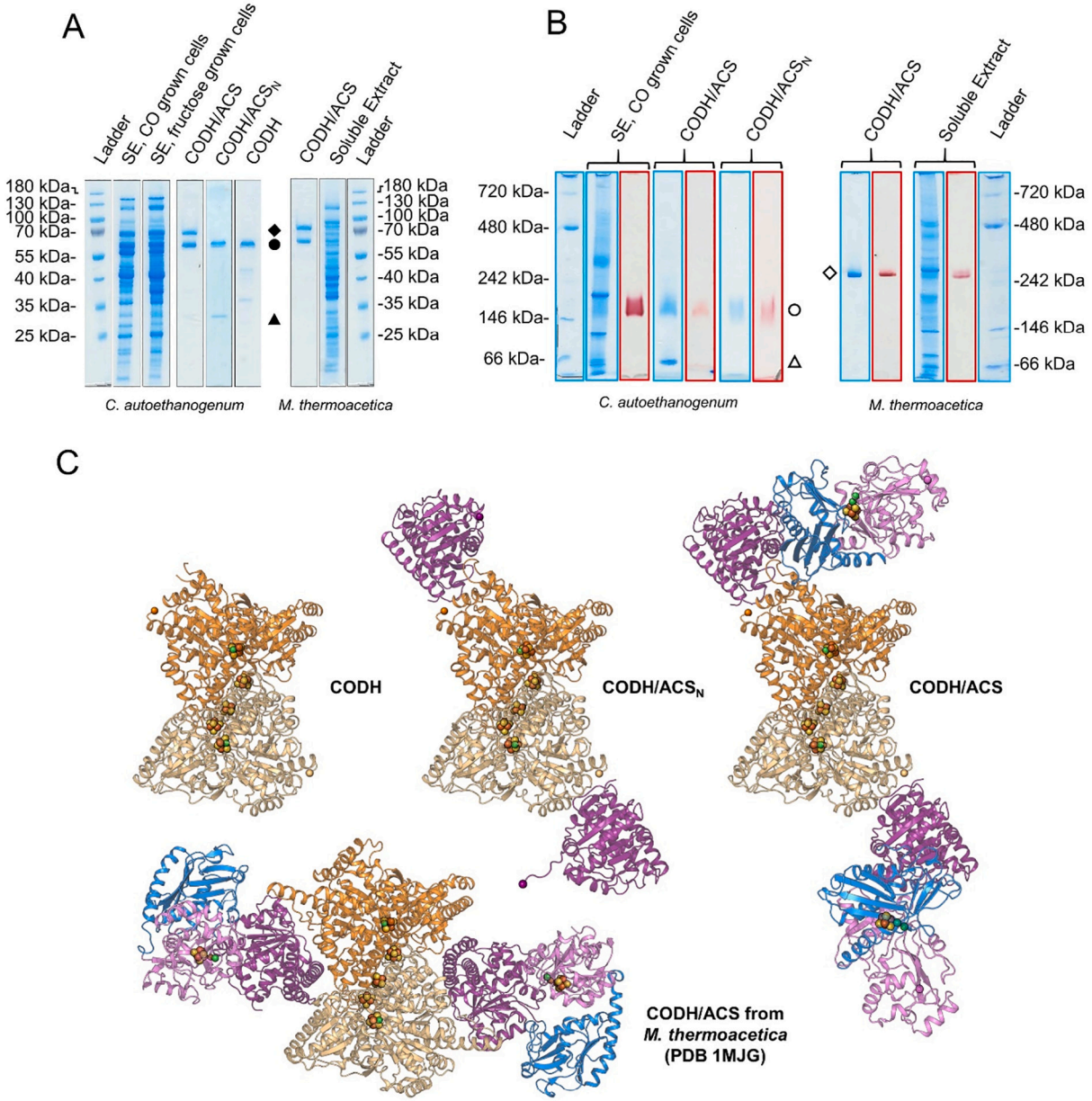

Fig. 2. SDS/Native PAGE profiles and structures of the CODH-containing complexes from *C. autoethanogenum* and *M. thermoacetica*. A. SDS PAGE profile of soluble extracts (SE) and natively purified CODH-containing complexes. Left: extracts after 140,000*g* ultracentrifugation obtained from CO-grown or fructose-grown *C. autoethanogenum*. *Ca*CODH/ACS and dimeric CODH were natively purified from both conditions, but the ones being presented here came from CO-grown cells. Limited proteolysis generated the CODH/ACS$_N$ (see Supplementary information). ◆: ACS; ●: CODH; ▲: ACS$_N$. Right: soluble extract and natively purified *Mt*CODH/ACS. B. hrCN PAGE and CODH activity staining of soluble extracts and pure complexes. Extracts are the same than in A, protein being stained by Coomassie (blue) or CODH activity (red). ◇: CODH/ACS; ○: CODH dimer; △: ACS. C. Structure of the different complexes obtained. The structure of *Mt*CODH/ACS obtained by Doukov et al. (PDB ID: 1MJG) [37] is shown in the same view to highlight structural differences. CODH is colored in light and deep orange. ACS is colored as in Fig. 1. (For interpretation of the references to color in this figure legend, the reader is referred to the web version of this article.)

[35]. The whole process was performed anaerobically in an anoxic chamber. Anaerobic fresh or frozen samples were used. Glycerol (20% v/v final) was added to each sample and 0.001% w/v Ponceau S serves as a marker for protein migration. The electrophoresis cathode buffer contained 50 mM Tricine; 15 mM Bis-Tris, pH 7; 0.05% w/v sodium deoxycholate; 0.01% w/v dodecyl maltoside and 2 mM of dithiothreitol (DTT). The anode buffer contained 50 mM Bis-Tris buffer pH 7 and 2 mM DTT. hrCN PAGE were carried out using a 5 to 15% linear polyacrylamide gradient and gels were run with a constant 40 mA current (PowerPac™ Basic Power Supply, Bio-Rad). After electrophoresis, protein bands were visualized by viologen-based CODH activity (see below) or with Instant Blue™ (Expedeon).

2.7. Mass spectrometric analysis

Coomassie stained band corresponding to *Ca*CODH was excised and analyzed by mass spectrometry. Briefly, cysteine residues of the protein were first in-gel reduced by dithiothreitol and alkylated by iodoacetamide and lysine residues were acylated by propionic anhydride. Then, the protein was in-gel digested overnight by AspN protease, the resulting

peptides extracted and dried down. Then the sample was reconstituted in 25 µL of 5% formic acid containing 5 fmol/µL retention time standard peptides (Pierce, Rockford, IL) and 5 µL were taken for LC-MS/MS analysis.

LC-MS/MS analysis was performed by MS Facility at the MPI-CBG Dresden, Germany, on a nano-UPLC Ultimate 3000 interfaced on-line to an Orbitrap HF hybrid mass spectrometer (both Thermo Fischer Scientific, Bremen). The UPLC system was equipped with Acclam PepMaptm 100 75 µm × 2 cm trapping column and 75 µm × 50 cm separating column packed with 3 µm C18 particles (Thermo Fischer Scientific, Bremen). Peptides were separated using 180 min linear gradients 0% to 65% of acetonitrile (solvent A – 0.1% formic acid in water, solvent B – 0.1% formic acid in neat acetonitrile). Spectra were acquired using Top20 data-dependent acquisition method, precursor *m/z* range was 350–1600 and dynamic exclusion time was 20 s. The lock-mass function was set to recalibrate MS1 scans using the background ion (Si(CH3)2O)6 at m/z 445.12. Acquired spectra were matched using MASCOT software (version 2.2.04). Mass tolerance was set on 5 ppm and 0.5 Da for precursor and fragment ions respectively; variable modification – cysteine carbamidomethyl, propionamide and sulfonic acid; methionine oxidation; lysine propionyl. The results were then manually inspected.

Altogether, more than 250 spectra were matched to the protein sequence providing 98% sequence coverage. More than 50 spectra were matched to AspN-specific or semi-specific overlapping peptides that covered sequencing stretch 390–416 with cysteine at the position 401.

2.8. Enzymatic assays

Enzymatic CODH activity measurements were performed in 50 mM potassium phosphate buffer, pH 8; 2 mM DTT. The rather alkaline pH was shown to be optimal for the *Mt*CODH/ACS activity [18] and we observed the same for the *Ca*CODH/ACS. Temperature was set to 50 °C, which is optimal for both enzymes. *Ca*CODH/ACS exhibits a slightly higher activity at this temperature than at 37 °C. A MV concentration of 5 mM was used, its reduction being spectrophotometrically followed at 600 nm on a Carry 60 spectrophotometer. The protein concentration in cuvettes ranged from 0.5 to 4 µg/mL. The molecular extinction coefficient of 15,489.6 $cm^{-1}{\cdot}M^{-1}$ was experimentally determined under these conditions and used for calculations. The reaction was initiated by the addition of 0.2 mL of 100% CO in an anaerobic quartz cuvette of 1.4 mL. Experiments were performed at least in triplicates. The indicated units refer to µmole of CO oxidized per minute. CODH activities from crude extracts were obtained from freshly harvested cells. In-gel viologen-based CODH activity staining was performed in 10 mL of anoxic 50 mM Tris-HCl buffer, pH 7.6; 2 mM DTT; 5 mM MV and 1 mM of 2,3,5-triphenyltetrazolium chloride. The latter component was used to maintain the staining under oxygen exposure. The native gels were loaded with 10 µg of soluble extracts or 1 µg of pure enzymes. Buffers and gels were anaerobically transferred in 1L-Duran Bottles and the gas phase was exchanged for 100% N_2 at 50 kPa. The reaction was started by the addition of 20 mL of 100% CO. Reaction were performed at 50 °C and stopped by opening the bottle under a fume hood.

CO production from purified CODH/ACS complexes was quantified in sealed anoxic 5 mL-Hungate tubes containing 1 mL of 50 mM potassium phosphate buffer, pH 8; 2 mM DTT and 0.01 g/L of anaerobic CODH/ACS. The gas phase was then exchanged for N_2/CO_2 (90:10%) with a final pressure of 100 kPa. The reaction was started by the addition of 10 mM of anaerobic titanium citrate as a reducing agent and performed at 50 °C. The CO concentration was quantified by gas chromatography, using column packed with Molecular Sieve 5 (Macherey & Nagel) connected to a HgO-to-Hg conversion detector (RGD2; Trace Analytical, Stanford, CA). The column was kept at 40 °C during separation, with synthetic air being used as the carrier gas at a flow rate of 32 mL/min. The CO concentration was calculated according to a CO standard. Generation of CO stayed linear during at least the first 4 h.

3. Results

3.1. Isolation of the CODH/ACS complex from C. autoethanogenum grown on CO or fructose

C. autoethanogenum was cultivated under either CO-autotrophic or heterotrophic conditions, respectively using CO or fructose as its main carbon and energy source. The acetogen is expected to use the Wood-Ljungdahl pathway under heterotrophic growth, fixing CO_2 generated by glycolysis and using the H_2 from the gas phase [4]. We therefore expected to detect the CODH/ACS and to natively and anaerobically purify the complex from both conditions. Accordingly, when comparing the SDS-PAGE protein profile of soluble extracts, only a few bands differ (Fig. 2A) and those corresponding to the purified complex, of a size of 67.9 and 76.9-kDa (according to the amino-acid sequence), are clearly visible. The complex subunits are apparently among the most expressed proteins. Their production is similar under both conditions, which is confirmed by CODH activity measurements with methyl viologen (21.3 ± 0.7 and 19.6 ± 0.6 units per mg of crude extract for heterotrophic and CO-autotrophic cultures, respectively, see table). Staining of the CODH activity from soluble extracts on hrCN PAGE showed a blurred band at an apparent size of 150-kDa (Fig. 2B). This size corresponds to the CODH dimer without the ACS, which is confirmed by the hrCN PAGE profile of the purified complex. Indeed, the latter exhibits two distinct bands, one at around 150-kDa, exhibiting CODH activity, and an activity-less lower band, corresponding to a size around 66-kDa (Fig. 2B). The complex thus migrates as a dimer of CODH (around 150-kDa) and monomers of ACS (around 77-kDa) in hrCN PAGE. However, size-exclusion chromatography (Supplementary Fig. S1) and the obtained structure (Fig. 2C) indicate a unique 292.45-kDa large (according to amino acid sequence and metal composition) $\alpha_2\beta_2$ biological unit in solution. The dissociation must therefore be driven by the electrophoretic conditions. It is worth noting here that a functional dimer of the same isoform of CODH, lacking ACS subunit, was also purified from both heterotrophic and CO conditions (Fig. 2A). However, this should be considered as a protein extraction artefact derived from an extensive sonication procedure that dissociated the complex. Indeed, a CODH lacking the ACS was not detected in extracts obtained by cell lysis in which the sonication step was omitted. Purified CODH/ACS and CODH were the only enzymes that exhibited detectable CODH activity with viologen dye in the extracts. Activity of the other CODH isoforms encoded by the genome was not detected during purification.

As a comparison, the acetogenic model organism *M. thermoacetica* was grown under heterotrophic conditions and its CODH/ACS complex was also natively purified (Fig. 2A, B). Contrarily to previous work

Table 1
Enzymatic activities of crude extracts and pure proteins. Activities were measured at 50 °C. CO-MV oxidoreductase activities were measured spectrophotometrically, CO production from CO_2 was measured *via* gas chromatography. For further details, see Materials and methods section.

Freshly extracted crude extracts	CODH activity with methyl viologen (µmol of CO oxidized/min/mg of total protein content)
C. autoethanogenum, heterotrophic growth on fructose	21.3 ± 0.7
C. autoethanogenum, autotrophic growth on CO	19.6 ± 0.6
M. thermoacetica, heterotrophic growth on fructose	1.10 ± 0.15

Pure enzymes, kept frozen	CODH activity with methyl viologen (µmol of CO oxidized/min/mg)	CO generated from CO_2 with titanium citrate (µmol of CO produced/min/mg)
*Ca*CODH/ACS	3.7 ± 0.8	0.240 ± 0.128
*Mt*CODH/ACS	6.4 ± 0.9	0.235 ± 0.072

[22,36,37], purification was performed using a heat-independent protocol to allow an analysis of the purified CODH/ACS obtained under comparable conditions. Activity of an isolated dimer of the CODH was not detected during purification, with or without sonication. Interestingly, SDS and hrCN PAGE profiles of extracts indicate that the CODH/ACS production is lower in *M. thermoacetica*, albeit using a similar metabolism than *C. autoethanogenum* under fructose-dependent growth [8] (Fig. 2A, B). Methyl viologen based CODH activity measurements confirmed this result, with an activity of only 1.10 ± 0.15 units per mg of crude extract (Table 1). Noteworthily, higher activities ranging from 10 to 15 units per mg were measured in other studies under similar heterotrophic conditions for *M. thermoacetica* and for the other model acetogen *Acetobacterium woodii* [18,38,39]. Thus, the production of *Mt*CODH/ACS was probably lowered due to our modified cultivation conditions. The *Mt*CODH/ACS complex migrates as a unique CODH activity-bearing unit on hrCN PAGE, with a size compatible with the 311.74-kDa $\alpha_2\beta_2$ organization [36] (Fig. 2B). Moreover, albeit both complexes exhibit a similar theoretical molecular weight (311.74 for *Mt*CODH/ACS and 292.45 kDa for *Ca*CODH/ACS, Supplementary Fig. S1), during size exclusion chromatography the elution volume of the *Mt*CODH/ACS complex is systematically lower than that of the *Ca*CODH/ACS enzyme, regardless of the column used. Biochemical and/or structural differences are expected between both complexes, causing the observed variation of Stokes radii.

Albeit *C. autoethanogenum* and *M. thermoacetica* are evolutionary closely related (both belonging to the *Clostridia* class) and use a similar energy metabolism, variations can be seen concerning the production and physicochemical properties of their CODH/ACS, the key enzyme of acetogenesis.

3.2. The CODH/ACS complex adopts an unforeseen binding mode in *C. autoethanogenum*

As freezing caused a drastic loss of the activity of the enzymes, as

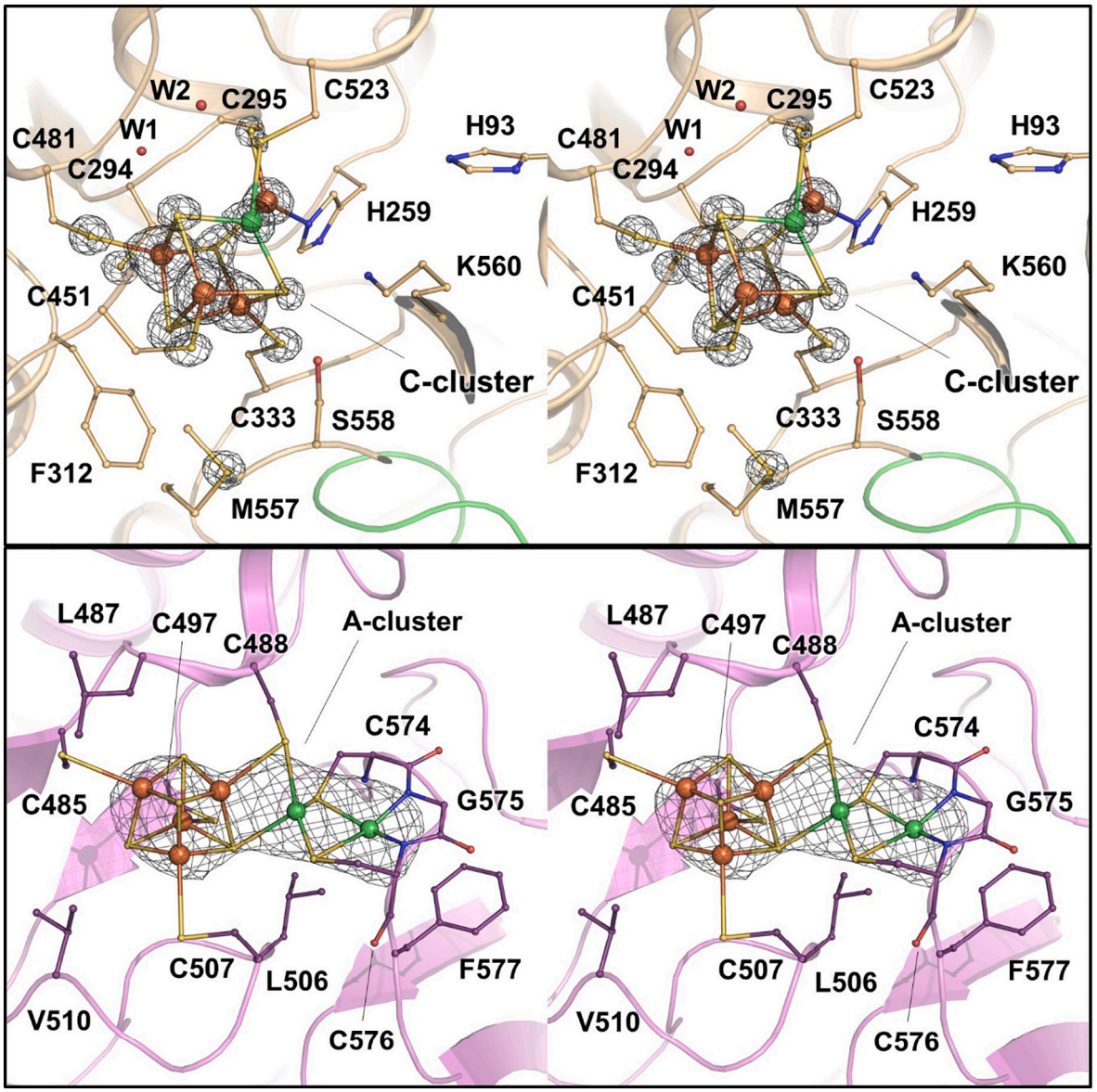

Fig. 3. Close-up of active sites of CODH and ACS of the *Ca*CODH/ACS complex. Stereo representation of the C-cluster (top panel) and A-cluster (bottom panel). The $2F_o$-F_c maps shown by a black mesh have been contoured at 7 and 5 σ for the C-cluster and A-cluster, respectively. Proteins are represented in cartoon. The clusters, surrounding residues and water molecules are shown in balls and sticks. Carbon atoms from the CODH and ACS are colored in light orange and light purple, respectively. Oxygen, nitrogen, sulfur, iron and nickel atoms are colored in red, blue, yellow, orange and green, respectively. (For interpretation of the references to color in this figure legend, the reader is referred to the web version of this article.)

already noticed with homologs [36], freshly purified proteins were immediately used for crystallization. Native *Ca*CODH/ACS, isolated from fructose or CO-grown cells, crystallized in a plethora of different precipitants, pH or additives. However, despite differences in the crystal morphology, the same crystalline form was systematically detected.

The overall crystal structure of the *Ca*CODH/ACS from fructose-grown cells was obtained at 3.0 Å (PDB ID: 6YTT) and contained one $\alpha_2\beta_2$ CODH/ACS complex in the asymmetric unit as previously shown in some crystallographic structures of the complex from *M. thermoacetica*. We also solved the *Ca*CODH/ACS from a CO-grown culture at 4.7 Å and despite the low-resolution, the electron density map perfectly matched the *Ca*CODH/ACS model obtained from the fructose-grown culture (Supplementary Fig. S2). We therefore conclude that both complexes are identical and contain the same CODH isoform (encoded by the CAETHG_1620–1621 locus).

The homodimeric CODH core is flanked by the ACS but with a

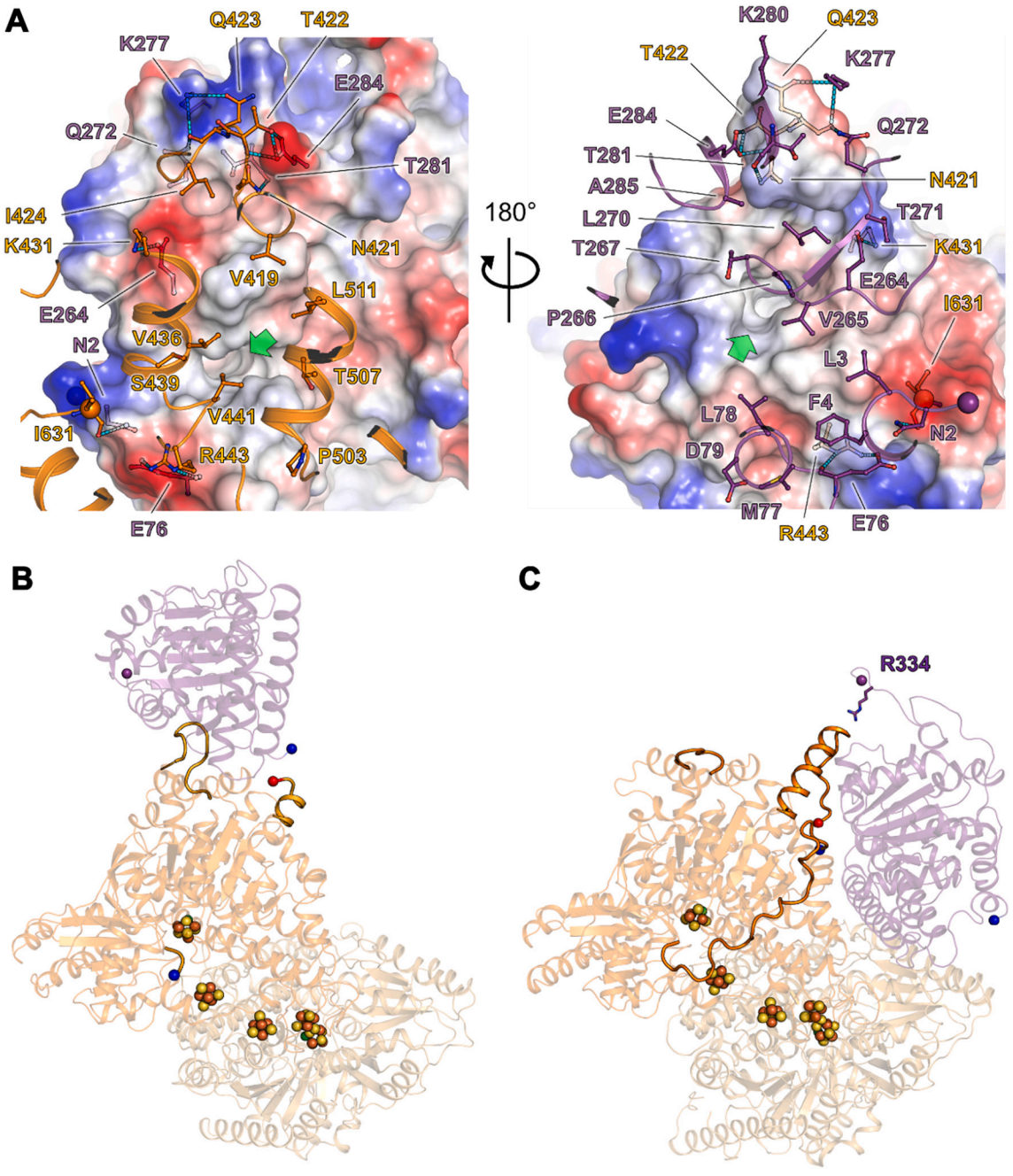

Fig. 4. Interaction of CODH and ACS subunits of *Ca*CODH/ACS compared to *Mt*CODH/ACS. A. Left panel, residues of CODH (orange) implicated in CODH interaction with ACS in *C. autoethanogenum*. Right panel, same view than the left panel turned at 180° to visualize residues of ACS (deep purple) implicated in the interaction with CODH. The residues are shown as balls and sticks with oxygen, nitrogen and sulfur atoms colored in red, blue and yellow, respectively. The CO-tunnel at the interface is pointed by a green arrow. The electrostatic transparent surface of the partner is colored in red and blue for the negative and positive charges, respectively. An orange sphere indicates the C-terminus of CODH, a purple one the N-terminus of the ACS. B, C. Comparison of the protein extensions implicated in CODH-ACS interaction in *Ca*CODH/ACS (B) and *Mt*CODH/ACS (PDB ID: 3I01) (C). N- and C-termini are represented by blue and red spheres. Only the N-terminal domain of the ACS is represented and its C-terminal connecting the next domain is shown as a purple sphere. The CODH dimer is colored in orange and light orange. Detailed sequence alignment is provided in Supplementary Fig. S6. The Arg334 of the *Mt*ACS is involved in a salt bridge with the CODH core and shown in stick. C-clusters and [Fe_4S_4] are shown as balls. (For interpretation of the references to color in this figure legend, the reader is referred to the web version of this article.)

strikingly different position compared to the enzyme of *M. thermoacetica* (Fig. 2C). The ACS unit, constituted of three juxtaposed domains, is found in two different conformations: a compact one, like the one from *M. thermoacetica*, and an extended one (Fig. 2C, Supplementary Fig. S3). The N-terminal domain is superposable in both conformations and well defined in the structure, exhibiting B-factors comparable to those of the CODH dimer core (Supplementary Figs. S3 and S4). Its central domain is highly flexible and barely seen in the structure, interacting with the C-terminal domain in the same fashion as other crystallized ACS [22,36,37]. The C-terminal domain containing the A-cluster is also highly disordered (Fig. 3 bottom panel and Supplementary Fig. S4) and the two last domains were mainly modelled based on the structural homologs [22,36,37]. The C-cluster was modelled accurately based on a higher resolution structure (see below, Fig. 3, top panel).

Since the whole complex of the *Mt*CODH/ACS is the only structural model known so far, the discovery of this new binding mode extends our vision on CODH/ACS complexes. To investigate if this new interface could be a crystallization artefact, structures obtained from other crystalline forms and packing are needed. We therefore screened different crystallization conditions, tried co-crystallization with putative ligands such as HS-CoA or acetyl-CoA to favor a different conformation of the ACS. Despite our efforts the same crystalline form was systematically obtained. Another strategy was therefore elaborated on the basis of the structural data. In *Ca*CODH/ACS, the flexibility between the N-terminal and the central domains of ACS derives from a poorly structured linker made of 28 residues (287–314). Its flexibility should make it an ideal target for proteolytic cleavage. Time-lapse limited proteolysis using trypsin, shown in Supplementary Fig. S5, indicated that in *Ca*CODH/ACS the CODH core is resistant to trypsin digestion, consistent with its compact structure, while the flexible ACS was extremely sensitive, as hypothesized. Anion-exchange chromatography allowed the separation of the degradation products in two main populations: A) the intact and active CODH core co-eluting with a 30-kDa protein (supposedly the N-terminal domain of ACS shortened as ACS_N in the text, Figs. 1 and 2, Supplementary Fig. S5) and B) a 50-kDa fragment with no apparent CODH activity (supposedly the central and C-terminal domains of ACS), contaminated with unproteolysed CODH/ACS complex (Supplementary Fig. S5). As a comparison, the compact ACS from *Mt*CODH/ACS is the most resistant part of the enzyme toward trypsin digestion, resulting in a completely different digestion profile and a quick loss of the CODH activity (Supplementary Fig. S5).

The fragment A was isolated *via* extra purification steps and crystallized. A new crystalline form was obtained, implicating different residues in crystalline packing, which diffracted to 3.14-Å resolution (PDB ID: 6YUA). The asymmetric unit contains a CODH dimer core with only the N-terminal domain fragment from the ACS and a part of the linker can be observed (Fig. 2C). The packing would not be compatible for the whole ACS since i) the whole complex would have an expected 32.3% of solvent content and ii) the presence of the whole ACS would induce many clashes. The crystal structure presented a similar position of the ACS N-terminal domain bound on the CODH and the contact interface is conserved (a rmsd of about 2 Å is observed between the ACS_N domains when the CODH core is superposed). This strengthened our assumptions about a new binding position of the ACS on the CODH core in *C. autoethanogenum*. The Fig. 4 highlights the differences of the CODH-ACS binding area between the two different acetogens. While the *Mt*CODH binds ACS on its CODH dimeric interface mainly *via* the N-terminal and a large C-terminal extension, only a monomer of *Ca*CODH interacts with its partner by an extended loop followed by an helix ranging from residues 420 to 440 for most part, conserved in the

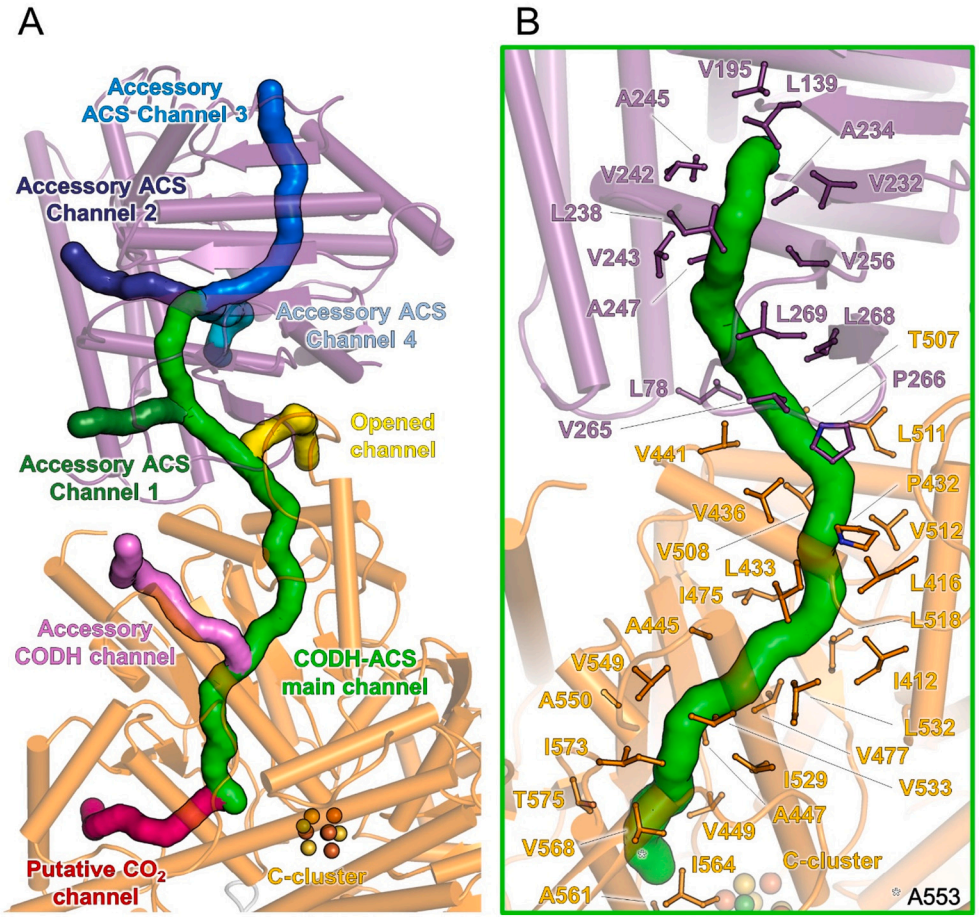

Fig. 5. Internal tunneling in *Ca*CODH/ACS. A. The hydrophobic channels in the *Ca*CODH/ACS structure, predicted by the CAVER program (with a probe radius of 1.2 Å), are highlighted by a surface representation. Proteins are colored as in Fig. 2C. The tunnels described in the text are indicated in different colors. A detailed view of each tunnel is given in Supplementary Fig. S8, tunnels predicted from each structure obtained in this study and *Mt*CODH/ACS are given in Supplementary Fig. S9. The middle and C-terminal domains of ACS were omitted to clarify the figure. B. Close up of the CODH/ACS main channel connecting the C-cluster to the ACS core. The residues forming the channel are shown in balls and sticks with nitrogen and oxygen atoms colored in blue and red, respectively. C-cluster is shown as balls with the iron, sulfur and nickel colored in orange, yellow and green, respectively. (For interpretation of the references to color in this figure legend, the reader is referred to the web version of this article.)

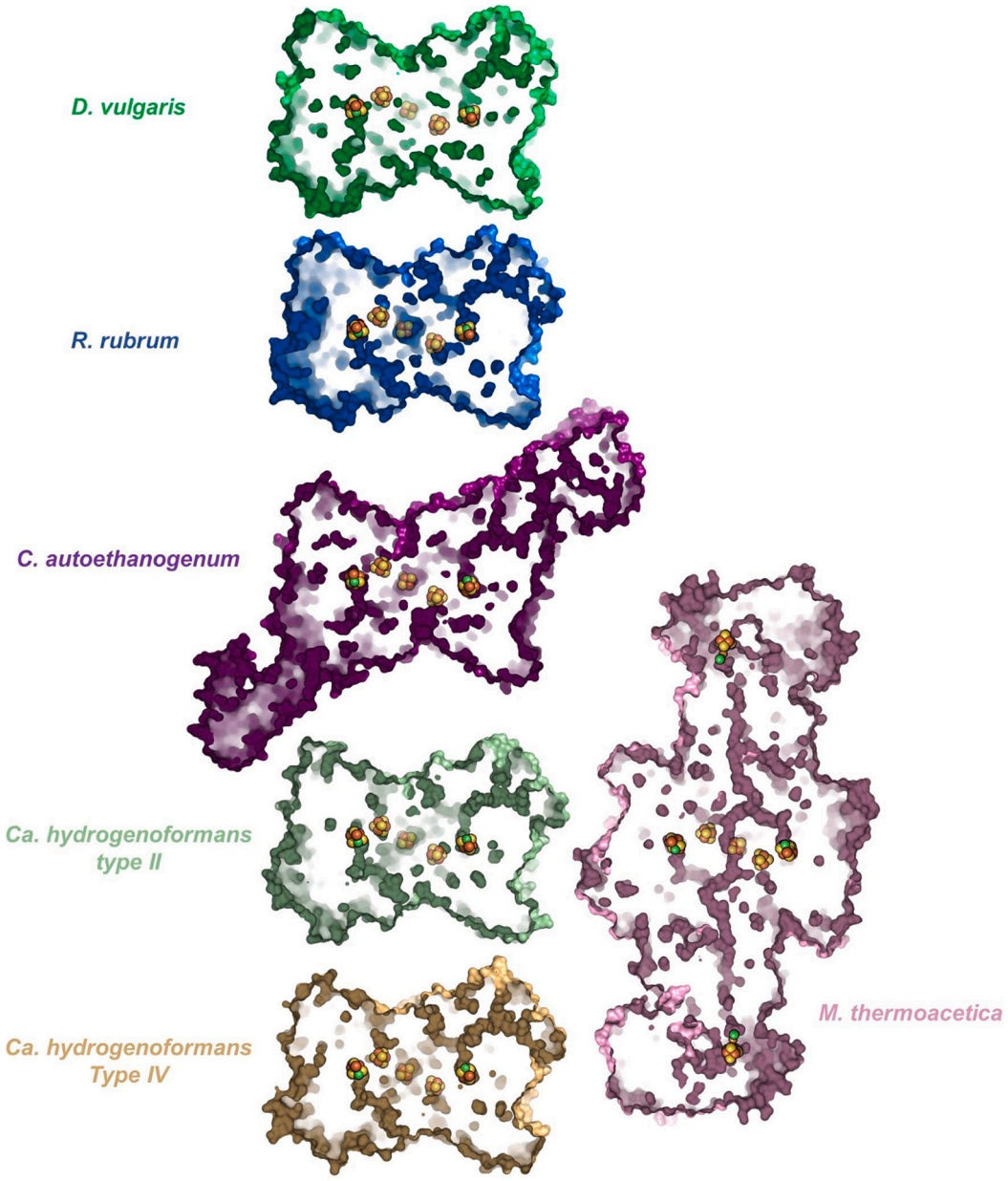

Fig. 6. Comparison of hydrophobic channels in the different structurally characterized CODH complexes. All models were superposed on the CODH dimer and shown with the same orientation. The surface of the proteins highlights the internal cavities. Metallo-clusters are shown as balls with the iron, sulfur and nickel colored in orange, yellow and green, respectively. Presented structures are, *D. vulgaris* (PDB ID: 6B6V) [42], *R. rubrum* (PDB ID: 1JQK) [43], *C. autoethanogenum* (PDB ID: 6YTT), *Ca. hydrogenoformans* type II (PDB ID: 1SU6) [44], *Ca. hydrogenoformans* type IV (PDB ID: 6ELQ) [40], and *M. thermoacetica* (PDB ID: 1MJG) [22]. (For interpretation of the references to color in this figure legend, the reader is referred to the web version of this article.)

Clostridiales order (*Clostridium* and *Acetobacterium* genus) but absent in other characterized CODH (Fig. 4, Supplementary Fig. S6). The resulting interface area would yield in a weaker interaction with an expected higher Kd. According to the PDBePISA server, in *Ca*CODH/ACS the interface CODH-ACS measures 1077.7 $Å^2$ ($\Delta G = -11.6$ kcal/mol) compared to 2319.8 $Å^2$ ($\Delta G = -14.2$ kcal/mol) in the case of *Mt*CODH/ACS. This difference could explain why the *Ca*CODH/ACS complex tends to dissociate during sonication and native electrophoresis, a feature that we did not observe for *Mt*CODH/ACS, as it could be due to an adaptation to thermophilic conditions. The natural abundance of CODH/ACS in *C. autoethanogenum* and the molecular crowding would ensure a stable complex within the cell.

3.3. A conserved C-cluster coordination for a different CO-channel network

The different binding interface between the CODH and ACS implies a reshuffling of the internal CO-network to transfer the CO from the C- to the A-clusters. In other words, if the *Ca*CODH has the same exact channel than *Mt*CODH, the entrance would be located on the surface, far away from the ACS. To precisely localize the CO-channels in the system of *C. autoethanogenum* we require a structure at higher resolution. Albeit being a fractionation artefact, we obtained the crystallographic structure of the CODH dimer (Fig. 2C) at 1.9 Å resolution (PDB ID: 6YU9).

The high quality of the electron density map allowed us to inspect the "read-through" stretch of the CODH. The gene coding for this enzyme seems to be interrupted by an internal TGA stop codon corresponding to

the residue position 401 that would separate the CODH in two peptides [19]. However, Liew et al. (2016) demonstrated that the gene is coding for one protein, reading through the stop codon [5]. Our studies confirmed this assumption based on SDS-PAGE (Fig. 2A). A mass spectrometry analysis showed the presence of a cysteine residue at position 401, coherent with the electron density and intriguingly different from the serine conserved in close *Clostridium* homologs (Supplementary Figs. S6 and S7). We did not detect any post-translational modification.

The structure offers a clear view of the C-cluster, composed of the canonical metallo-cofactor Fe-[$NiFe_3S_4$], which has already been described in several studies [36,40–44]. The position in front of the Ni seems vacant or partially occupied by a ligand, modelled as a water molecule. Our data does not support the presence of a bound sulfido-ligand as previously reported in the high resolution CODH type II isoform from *Ca. hydrogenoformans* [44]. In *C. autoethanogenum* the C-cluster is coordinated by the Cys 295, 333, 451, 481 and 523 and His 259. The surrounding environment is almost identical compared to other systems (Fig. 3, top panel, Supplementary Fig. S6).

The localization of the channels in the *C. autoethanogenum* complex was performed by the software CAVER [34]. As predicted by the ACS position, the CO channels differ completely between *Mt*CODH/ACS and *Ca*CODH/ACS (Figs. 5, 6, Supplementary Figs. S8, S9 and S10). Three hydrophobic channels devoid of any water molecules were detected in the *Ca*CODH (Fig. 5 and Supplementary Fig. S9 panel A). The main channel, the longest and most prominent one, is crossing through both, the CODH and the ACS, and links the C-cluster to the N-terminal domain of ACS. It is therefore the functional equivalent of the CO-tunnel in *Mt*CODH/ACS. A shorter tunnel (Putative CO_2 channel, Fig. 5) connects the C-cluster to the surface of the CODH and might be important for CO_2 accessibility to the C-cluster. The last one (Accessory CODH channel, Fig. 5) emanates from the main channel and extrudes to the surface instead of joining the ACS. Contrarily to *M. thermoacetica*, the C-clusters are connected by a fully hydrated and polar cavity, which would restrain a CO-internal transfer between C-clusters [36]. Interestingly, the enzyme of *C. autoethanogenum* exhibits a tunneling system that is more similar to those present in stand-alone CODH, such as the one structurally characterized from *Ca. hydrogenoformans* (PDB ID: 6ELQ and 1SU6 [40,44]), *Desulfovibrio vulgaris* (PDB ID: 6B6V [42]) or *Rhodospirillum rubrum* (PDB ID: 1JQK [43]) (Fig. 6). This result suggests that the *Ca*CODH is evolutionarily closer to these stand-alone enzymes than to *Mt*CODH. Sequence alignment and the generated phylogenetic tree further support this assumption (Supplementary Fig. S6).

The main channel, which connects both subunits, is also not completely sealed and opens at the interface between the CODH and the ACS (Opened channel, Fig. 5). Even if the opening of accessory channels would be large enough to release CO, the hydrophobic environment might still serve as a conducting platform to funnel the CO toward the ACS. Despite a resolution of 3.01 Å, numerous features could be extrapolated from the ACS N-terminal part of the *Ca*CODH/ACS structure. The central channel, coming from the CODH, propagates in the ACS N-terminal domain and splits in two routes, of which one has immediate access to the solvent (accessory ACS channel 1), while the second one joins the core of the N-terminal domain. At this center, the channel splits again into three cavities which are connected to the solvent and surrounded by hydrophobic residues (accessory ACS channels 2, 3 and 4, Fig. 5 and Supplementary Figs. S8 and S9). While the accessory channels 1 and 4 seem to be an additional porous network, the channels 2 and 3 have similarities with *Mt*ACS. For instance, the accessory channel 2 superposes with the main gas channel of the *Mt*CODH/ACS that connects the C-cluster to the *Mt*ACS core (Supplementary Fig. S10). A part of the accessory channel 3 follows the same direction than the CO-channel by connecting the core of *Mt*ACS to the A-cluster harbored by the C-terminal domain and therefore might perform the same function, albeit requiring a spatial readjustment to fit the channel exit. Under CO-autotrophic growth the porous network might allow the CO to freely diffuse inside the enzyme but it could be a disadvantage when the complex must cope with CO_2-reduction to form acetyl-CoA.

3.4. C-cluster accessibility is independent of the internal channeling

In order to ascertain if the porous network is a biological reality in solution, we compared CO-oxidation and CO-production rates of purified CODH/ACS complexes from both acetogens. CODH activity measurements, monitored by MV reduction, indicate that *Mt*CODH/ACS is around two-fold more active than *Ca*CODH/ACS (6.4 ± 0.9 and 3.7 ± 0.8 units per mg of frozen enzyme, respectively, see Table 1) under the same experimental conditions. Beside the difference in activities, these measurements also suggest that the C-clusters are accessible to external CO in both enzymes. This result aligns with previous work which showed that *Mt*CODH/ACS catalyzes the direct or indirect interconversion of CO and acetyl-CoA and thus incorporates CO [45,46]. Furthermore, the CODH activity of the functional dimer of CODH from *C. autoethanogenum* that we purified (5.3 ± 0.7 units per mg of frozen enzyme) suggests that there is no impairment of CO diffusion to the C-cluster in the whole complex, as the CODH exhibits roughly the same activity in the presence or the absence of ACS. In the reverse direction, we monitored CO_2-to-CO reduction by using titanium citrate as reductive agent and the CO released was quantified *via* gas chromatography. Like for the oxidation reactions, our assays indicate that both enzymes generate CO at rates in a similar order of magnitude (0.240 ± 0.128 and 0.235 ± 0.072 μmol of CO produced/min/mg of frozen *Ca*CODH/ACS and *Mt*CODH/ACS, respectively, see Table 1). Despite the structural data indicating a robust and sealed internal tunnel in *Mt*CODH/ACS and a leaky tunneling system in *Ca*CODH/ACS, both enzymes behave like stand-alone CODH with accessible C-clusters under such experimental conditions.

4. Discussion and conclusions

4.1. An identical overall reaction for a singular organization

CODH/ACS are considered as ancestral enzymes [47]. They have the fundamental role of performing acetyl-CoA production, the main precursor for carbon-based anabolic processes during autotrophic growth. Therefore, it could be assumed that these enzymes are perfectly conserved across organisms which use the Wood-Ljungdahl pathway. However, despite a conserved mechanism and similar structure, many subtleties emerged during evolution. In methanogenic archaea for instance, a super complex made of the CODH/ACS, the methyl-tetrahydromethanopterin methyltransferase and the corrinoid FeS containing protein is able to directly convert a methyl-group (carried by tetrahydromethanopterin), CO_2 and HS-CoA into acetyl-CoA by the use of reduced ferredoxin [14,48]. Here we show that even among the *Clostridia* class large disparities exist. *Mt*CODH/ACS was the canonical structural model because it was the only whole complex described so far. Its organization reflects a compact and stable structure with a sealed CO-channel. In contrast, the crystal structure of *Ca*CODH/ACS shows a different oligomeric arrangement and multiple solvent-accessible tunnels, reaching to both active sites. Our limited proteolysis experiments indicate major differences concerning the accessibility of *Mt*ACS and *Ca*ACS for proteases, which would derive from a natural flexibility of the *Ca*ACS but also from a rigidification toward a thermophilic adaptation of *M. thermoacetica*.

The intrinsic disorder in the ACS is puzzling and one can wonder why the enzyme from *C. autoethanogenum* has such high degree of flexibility. Our main hypothesis is that the ACS needs a trigger in solution to switch to a transient catalytic state. Co-crystallization in presence of HS-CoA or acetyl-CoA systematically provided the same crystalline form with the same overall conformation. This observation could come from a trapped given conformation under the crystallization conditions or HS-CoA does not trigger any conformational switch. In the last scenario, the protein

would be in a flexible standing state until interacting with the methyl-loaded corrinoid FeS protein partner, the ACS then closing the active site. The binding area between both would allow a dramatic rearrangement. The intrinsic flexibility of the ACS could thus favor the exchange of partners and stimulate the turn-over toward acetyl-CoA formation. This flexible "standing" state would explain the accessibility of the C-cluster to CO/CO_2 that was detected by our activity measurements. Albeit crystallographic structures indicate a sealed CO tunnel in *Mt*CODH/ACS, CO-formation/consumption was measured at similar rates in solution (Table 1). We therefore hypothesize a flexible ACS in solution, while the crystallization process "traps" only a rigid conformation for *Mt*CODH/ACS. It would explain the few structures exhibiting different ACS conformations [36,49] (Supplementary Fig. S3), while the evidence for the existence of a sealed CO-tunnel in solution for *Mt*CODH/ACS was obtained in the presence of the partners, which could induce the closed conformation [23].

4.2. CO-channels reshuffling to facilitate CO diffusion

From CAVER analyses eight hydrophobic channels have been detected in *Ca*CODH/ACS (Fig. 5 and Supplementary Figs. S8 and S9). This profusion could be caused by the physiological plasticity of the acetogen. Contrary to the closely related *Ca. hydrogenoformans*, which uses different monodirectional CODH to specifically perform high-rate CO-oxidation (stand-alone CODH) and acetyl-CoA synthesis (CODH/ACS complex) [24], *C. autoethanogenum* uses a single CODH/ACS complex under all tested growth conditions.

Based on our results we suggest that under fructose-grown conditions or autotrophy on H_2 and CO_2 the complex couples CO_2-reduction to acetyl-CoA biosynthesis. Under such conditions, CO would be funneled to the A-cluster by the main channel, like in *Mt*CODH/ACS. The putative CO_2-channel (Fig. 5, in red) would efficiently and specifically feed the C-cluster with CO_2. With a rapid turn-over at the A-cluster, the tunnel hydrophobicity should be enough to trap CO without significant leakage. However, if the acetyl-CoA synthesis rate becomes limiting, porosity of the enzyme would be disadvantageous, as CO leakage represents a loss of crucial low potential electrons. This might explain the hurdle to cultivate *C. autoethanogenum* on H_2 and CO_2, since the organism uses an energy limited metabolism in which any energy loss is dramatic [5]. However, in the presence of external CO, the condition used for isolation of the bacterium, the porosity of the enzyme should be a selective advantage. In *M. thermoacetica*, an external CO concentration exceeding 50 μM impairs internal channeling, decreasing the acetyl-CoA synthesis by 90% [50]. The remaining 10% activity is stable while the CO concentration increases and is comparable to the activity of an isolated ACS subunit, which directly incorporates CO [50]. Thus, excessive CO concentrations make the CODH unnecessary for acetyl-CoA synthesis. This explains the production of monomeric ACS by *Ca. hydrogenoformans* during CO-autotrophic growth, in addition to the CODH/ACS complex [51]. Supposing that such inhibition also exists in *C. autoethanogenum*, the open tunnels of *Ca*CODH/ACS would represent a way to release the inhibiting CO-excess from the tunnels and to make the A-cluster accessible to external CO. The complex would be used for detoxification, carbon assimilation and energy production, channeling the CO toward both: to the C-cluster for fast oxidation and to the A-cluster to branch CO and produce acetyl-CoA (Fig. 7). Under these conditions, the usage of the accessory CODH channel (pink, Fig. 5) and the opening between both subunits (yellow, Fig. 5) would stimulate CO-diffusion in the CODH while the evacuation of the CO_2 would be still assured by the putative CO_2 channel (red, Fig. 5).

Noteworthily, the negative impact of a porous *Ca*CODH/ACS to channel CO toward acetyl-CoA formation under CO_2-conditions could still be counterbalanced at the cellular level by partners, metabolites or regulators, which might affect channels openture. Such regulators could have been lost during the purification procedure.

4.3. The CODH/ACS as a main CO-conversion nano-machine

Under CO-growth, the highly produced all-in-one *Ca*CODH/ACS complex provides cellular energy and building blocks for anabolism. On one hand, CODH captures and oxidizes CO at a high rate, releasing CO_2 and reducing ferredoxin. For metabolic needs, ferredoxins will be

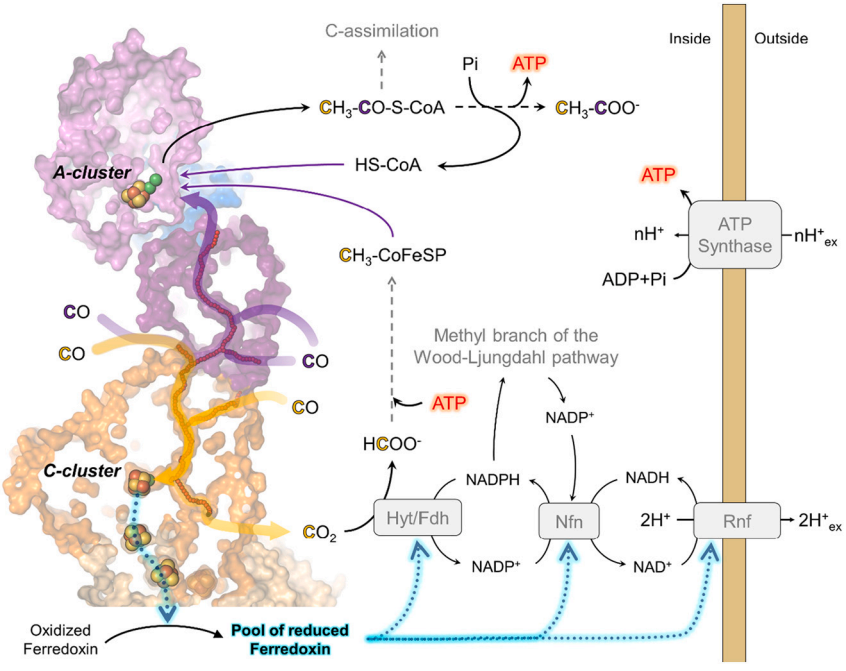

Fig. 7. Schematic representation of the central bidirectional role of CODH/ACS complex from *C. autoethanogenum* during autotrophic CO growth. *Ca*CODH/ACS is represented by its surface and colored as in Fig. 2C. Cofactors are represented in spheres with iron, sulfur and nickel colored in orange, yellow and green, respectively. Gas diffusion in internal tunnels are visualized by orange and purple arrows, depending on the implicated subunit. In CO-autotrophic growth, the reduced ferredoxins generated by CO-oxidation at the C-cluster are necessary for ion translocation (and thus energy production), NADH and NADPH generation and CO_2 reduction into formate ($HCOO^-$) [8,14]. The latter will be condensed, dehydrated, reduced, and transferred to ultimately form a methyl-group on the corrinoid-FeS protein (CoFeSP, C_1-carrier) by the methyl branch of the Wood-Ljungdahl pathway, consuming NADPH [9,14]. The electron donor for the second reduction step in the Wood-Ljungdahl pathway of *C. autoethanogenum* is still unclear [4,8] and not indicated. The methyl group is then combined at the A-cluster with HS-CoA and CO, to synthesize acetyl-CoA. This latter can be derived for anabolism but most of the generated acetyl-CoA is used by the organism to produce acetate (and then ethanol and 2, 3-butanediol), allowing ATP regeneration. The stoichiometry of the reactions is not respected to simplify the scheme. (For interpretation of the references to color in this figure legend, the reader is referred to the web version of this article.)

directly oxidized for I) NADH and membrane gradient formation (Rnf system), II) NADPH generation (Nfn system) and III) CO_2-reduction through the Wood-Ljungdahl pathway (*e.g.* Hyt/Fdh complex) [3,8,14,52–54] (Fig. 7). On the other hand, the acetyl-CoA synthase will combine external CO to the methyl-group generated by the Wood-Ljungdahl pathway and HS-CoA to make acetyl-CoA. The latter will be transformed to acetate, ethanol or 2, 3-butanediol [6,7,9] or will enter in the central-carbon metabolism. If other acetogens can thrive using CO, the whole metabolism of *C. autoethanogenum* is designed for a highly efficient gas conversion.

4.4. A new structural prototype to unveil the evolution of a primordial enzyme

With the discovery of a novel CODH/ACS organization our work provides new perspectives on the variability which exists even among crucial and conserved enzymatic complexes. Further work is necessary to understand why *C. autoethanogenum* developed such a different complex, despite belonging to the same bacterial class than *M. thermoacetica*. Adaptation to a CO-rich environment should be one of the main reasons. Anaerobic bacteria can use different strategies to cope with autotrophic growth on CO, while still being dependent on a [Ni—Fe]-containing CODH. In comparison to *Ca. hydrogenoformans*, which contains five isoforms of the CODH in its genome of which all appear to be dedicated to monodirectional reactions [24], the evolution of *C. autoethanogenum* and probably related *Clostridium* species shaped an enzyme that is performant under all CO concentrations. Another interesting feature is that our structural results, sequence alignments and phylogenetic studies indicate that the *Ca*CODH is phylogenetically closer to the structurally characterized stand-alone CODH, including those of *Ca. hydrogenoformans*, than to *Mt*CODH (Fig. 6; Supplementary Fig. S6). One can suspect a constant source of surprises regarding the evolution of the CODH subunit, as already pointed out by previous work [55–57]. Evolutive convergence could also be expected. Indeed, when compared to the unique structure of a methanogenic CODH (PDB ID: 3CF4 [58]), it seems that the CO cavity in front of the C-cluster follows the same orientation than the one from *Ca*CODH/ACS (Supplementary Fig. S11, top panels). Which rises the following question: does the archaeal ACS share the same fixation point than the one from *C. autoethanogenum*? When the CODH core of the archaeal model and *Mt*CODH/ACS are superposed (Supplementary Fig. S11, bottom panels), numerous clashes exist between the *Mt*ACS and the epsilon subunit as well as archaeal CODH extensions containing extra $[Fe_4S_4]$-clusters. If the same superposition is performed with *Ca*CODH/ACS, the ACS part would sit in front of the CO-cavity in the archaeal model and generate only a minor clash at the C-terminal helix position of the CODH. Phylogenetic analyses discarded the possibility of an Archaea-*C. autoethanogenum* horizontal transfer (Supplementary Fig. S6), as previously shown [24,56,57]. If the necessity to modify the tunnel orientation in the archaeal enzyme could be explained by the additional subunits and CODH extensions, the reasons for a convergent evolution of *Ca*CODH/ACS are still elusive. Until additional structural data is available the features of the archaeal CODH-ACS interface will be speculative, as the absence of the N-terminal domain in the ACS from *Methanosarcinales* complicates hypotheses about possible interactions even more. One could suspect that the *Ca*CODH/ACS channeling system is more ancient and common than the one from the *Mt*CODH/ACS, specialized for CO_2-reduction.

If a model such as *C. autoethanogenum*, among the well-studied *Clostridium* genus, can exhibit this specialized CODH/ACS complex, one can wonder: are there more different CODH-containing systems out there? Exploring the natural diversity of other models, even among closely-related ones, will not only provide us with more templates to develop bio-catalysts, it will seize the variability and provide clues how evolution shaped these enzymes to match the required physiological needs.

Declaration of competing interest

The authors declare that they have no known competing financial interests or personal relationships that could have appeared to influence the work reported in this paper.

Acknowledgements

We would like to deeply thank Christina Probian for her continuous help that allowed the elaboration of this project and Marion Jespersen for her critical comments and deep reviewing of the manuscript. We acknowledge the Max Planck Institute for Marine Microbiology for continuous support. We thank the staff of beamline P13 from the EMBL at PETRA III, Proxima 1 from SOLEIL and PXIII from SLS. We especially acknowledge Dr. Pierre Legrand for his advices concerning Staraniso, and Dr. Sylvain Engilberge for his help with the tentative of Xenon derivatization on *Ca*CODH/ACS crystals and data collection on PXIII at the SLS. We thank the MS Facility at MPI CBG, Dresden, for MS-analysis of the protein, and especially Anna Shevchenko for her help and fruitful comments. We also would like to acknowledge the National Oceanic and Atmospheric Administration (NOAA) photo library for providing not copyrighted images such the one we used for graphical abstract (Black Smoker; Image courtesy of NOAA Office of Ocean Exploration and Research, 2016 Deepwater Exploration of the Marianas). We acknowledge the Pexels database for the royalty-free images they provide, as the one we used for the graphical abstract (Factory photography by Chris LeBoutillier).

Funding sources

This work was funded by the Max-Planck-Gesellschaft and the Deutsche Forschungsgemeinschaft priority program 1927, “Iron-Sulfur for Life” WA 4053/1-1.

Appendix A. Supplementary data

Supplementary data to this article can be found online at https://doi.org/10.1016/j.bbabio.2020.148330.

References

[1] P.R.F. Cordero, K. Bayly, P. Man Leung, C. Huang, Z.F. Islam, R.B. Schittenhelm, G. M. King, C. Greening, Atmospheric carbon monoxide oxidation is a widespread mechanism supporting microbial survival, ISME J. 13 (2019) 2868–2881, https://doi.org/10.1038/s41396-019-0479-8.

[2] F.T. Robb, S.M. Techtmann, Life on the fringe: microbial adaptation to growth on carbon monoxide, F1000Res. 7 (2018), https://doi.org/10.12688/f1000research.16059.1.

[3] S. Wang, H. Huang, J. Kahnt, A.P. Mueller, M. Kopke, R.K. Thauer, NADP-specific electron-bifurcating [FeFe]-hydrogenase in a functional complex with formate dehydrogenase in *Clostridium autoethanogenum* grown on CO, J. Bacteriol. 195 (2013) 4373–4386, https://doi.org/10.1128/JB.00678-13.

[4] J. Mock, Y. Zheng, A.P. Mueller, S. Ly, L. Tran, S. Segovia, S. Nagaraju, M. Kopke, P. Durre, R.K. Thauer, Energy conservation associated with ethanol formation from H_2 and CO_2 in *Clostridium autoethanogenum* involving electron bifurcation, J. Bacteriol. 197 (2015) 2965–2980, https://doi.org/10.1128/JB.00399-15.

[5] F. Liew, A.M. Henstra, K. Winzer, M. Kopke, S.D. Simpson, N.P. Minton, Insights into CO_2 Fixation Pathway of *Clostridium autoethanogenum* by Targeted Mutagenesis, MBio 7, 2016, https://doi.org/10.1128/mBio.00427-16.

[6] J. Abrini, H. Naveau, E.-J. Nyns, *Clostridium autoethanogenum*, sp. nov., an anaerobic bacterium that produces ethanol from carbon monoxide, Archives of Microbiology 161 (1994) 345–351, https://doi.org/10.1007/BF00303591.

[7] E. Marcellin, J.B. Behrendorff, S. Nagaraju, S. DeTissera, S. Segovia, R. W. Palfreyman, J. Daniell, C. Licona-Cassani, L.-e. Quek, R. Speight, M.P. Hodson, S.D. Simpson, W.P. Mitchell, M. Köpke, L.K. Nielsen, Low carbon fuels and commodity chemicals from waste gases – systematic approach to understand energy metabolism in a model acetogen, Green Chem. 18 (2016) 3020–3028, https://doi.org/10.1039/C5GC02708J.

[8] K. Schuchmann, V. Müller, Autotrophy at the thermodynamic limit of life: a model for energy conservation in acetogenic bacteria, Nat. Rev. Microbiol. 12 (2014) 809–821, https://doi.org/10.1038/nrmicro3365.

[9] J.K. Heffernan, K. Valgepea, R. de Souza Pinto Lemgruber, I. Casini, M. Plan, R. Tappel, S.D. Simpson, M. Köpke, L.K. Nielsen, E. Marcellin, Enhancing CO_2-

valorization using *Clostridium autoethanogenum* for sustainable fuel and chemicals production, Frontiers in Bioengineering and Biotechnology 8 (2020), https://doi.org/10.3389/fbioe.2020.00204.
[10] H.L. Drake, A.S. Gossner, S.L. Daniel, Old acetogens, new light, Ann. N. Y. Acad. Sci. 1125 (2008) 100–128, https://doi.org/10.1196/annals.1419.016.
[11] L.G. Ljungdahl, A life with acetogens, thermophiles, and cellulolytic anaerobes, Annu. Rev. Microbiol. 63 (2009) 1–25, https://doi.org/10.1146/annurev.micro.091208.073617.
[12] S. Menon, S.W. Ragsdale, Evidence that carbon monoxide is an obligatory intermediate in anaerobic acetyl-CoA synthesis, Biochemistry 35 (1996) 12119–12125, https://doi.org/10.1021/bi961014d.
[13] J.C. Xavier, M. Preiner, W.F. Martin, Something special about CO-dependent CO_2 fixation, FEBS J. 285 (2018) 4181–4195, https://doi.org/10.1111/febs.14664.
[14] O.N. Lemaire, M. Jespersen, T. Wagner, CO_2-Fixation Strategies in Energy Extremophiles: What Can We Learn From Acetogens?, Frontiers in Microbiology 11, 2020, https://doi.org/10.3389/fmicb.2020.00486.
[15] M. Can, F.A. Armstrong, S.W. Ragsdale, Structure, function, and mechanism of the nickel metalloenzymes, CO dehydrogenase, and acetyl-CoA synthase, Chem. Rev. 114 (2014) 4149–4174, https://doi.org/10.1021/cr400461p.
[16] B.P. Tracy, S.W. Jones, A.G. Fast, D.C. Indurthi, E.T. Papoutsakis, *Clostridia*: the importance of their exceptional substrate and metabolite diversity for biofuel and biorefinery applications, Curr. Opin. Biotechnol. 23 (2012) 364–381, https://doi.org/10.1016/j.copbio.2011.10.008.
[17] J.R. Phillips, E.C. Clausen, J.L. Gaddy, Synthesis gas as substrate for the biological production of fuels and chemicals, Appl. Biochem. Biotechnol. 45 (1994) 145–157, https://doi.org/10.1007/BF02941794.
[18] S.W. Ragsdale, J.E. Clark, L.G. Ljungdahl, L.L. Lundie, H.L. Drake, Properties of purified carbon monoxide dehydrogenase from *Clostridium thermoaceticum*, a nickel, iron-sulfur protein, J. Biol. Chem. 258 (1983) 2364–2369.
[19] S.D. Brown, S. Nagaraju, S. Utturkar, S. De Tissera, S. Segovia, W. Mitchell, M. L. Land, A. Dassanayake, M. Köpke, Comparison of single-molecule sequencing and hybrid approaches for finishing the genome of *Clostridium autoethanogenum* and analysis of CRISPR systems in industrial relevant *Clostridia*, Biotechnol. Biofuels 7 (2014) 40, https://doi.org/10.1186/1754-6834-7-40.
[20] J. Shin, Y. Song, Y. Jeong, B.-K. Cho, Analysis of the Core Genome and Pan-Genome of Autotrophic Acetogenic Bacteria, Frontiers in Microbiology 7, 2016, https://doi.org/10.3389/fmicb.2016.01531.
[21] S.W. Ragsdale, E. Pierce, Acetogenesis and the Wood-Ljungdahl pathway of CO_2 fixation, Biochim. Biophys. Acta 1784 (2008) 1873–1898, https://doi.org/10.1016/j.bbapap.2008.08.012.
[22] T.I. Doukov, L.C. Blasiak, J. Seravalli, S.W. Ragsdale, C.L. Drennan, Xenon in and at the end of the tunnel of bifunctional carbon monoxide dehydrogenase/acetyl-CoA synthase, Biochemistry 47 (2008) 3474–3483, https://doi.org/10.1021/bi702386t.
[23] E.L. Maynard, P.A. Lindahl, Evidence of a molecular tunnel connecting the active sites for CO_2 reduction and acetyl-CoA synthesis in acetyl-CoA synthase from *Clostridium thermoaceticum*, J. Am. Chem. Soc. 121 (1999) 9221–9222, https://doi.org/10.1021/ja992120g.
[24] S.M. Techtmann, A.S. Colman, M.B. Murphy, W.S. Schackwitz, L.A. Goodwin, F. T. Robb, Regulation of multiple carbon monoxide consumption pathways in anaerobic bacteria, Front. Microbiol. 2 (2011) 147, https://doi.org/10.3389/fmicb.2011.00147.
[25] W. Kabsch, Integration, scaling, space-group assignment and post-refinement, Acta Crystallogr. D Biol. Crystallogr. 66 (2010) 133–144, https://doi.org/10.1107/S0907444909047374.
[26] M.D. Winn, C.C. Ballard, K.D. Cowtan, E.J. Dodson, P. Emsley, P.R. Evans, R. M. Keegan, E.B. Krissinel, A.G.W. Leslie, A. McCoy, S.J. McNicholas, G. N. Murshudov, N.S. Pannu, E.A. Potterton, H.R. Powell, R.J. Read, A. Vagin, K. S. Wilson, Overview of the CCP4 suite and current developments, Acta Crystallogr. D Biol. Crystallogr. 67 (2011) 235–242, https://doi.org/10.1107/S0907444910045749.
[27] I.J. Tickle, C. Flensburg, P. Keller, W. Paciorek, A. Sharff, C. Vonrhein, G. Bricogne, STARANISO. http://staraniso.globalphasing.org/cgi-bin/staraniso.cgi, Global Phasing Ltd., Cambridge, United Kingdom, .
[28] I. Usón, G.M. Sheldrick, An introduction to experimental phasing of macromolecules illustrated by SHELX; new autotracing features, Acta Crystallogr. D Biol. Crystallogr. 74 (2018) 106–116, https://doi.org/10.1107/S2059798317015121.
[29] D. Liebschner, P.V. Afonine, M.L. Baker, G. Bunkóczi, V.B. Chen, T.I. Croll, B. Hintze, L.W. Hung, S. Jain, A.J. McCoy, N.W. Moriarty, R.D. Oeffner, B.K. Poon, M. G. Prisant, R.J. Read, J.S. Richardson, D.C. Richardson, M.D. Sammito, O.V. Sobolev, D.H. Stockwell, T.C. Terwilliger, A.G. Urzhumtsev, L.L. Videau, C.J. Williams, P.D. Adams, Macromolecular structure determination using X-rays, neutrons and electrons: recent developments in Phenix, Acta Crystallogr. D 75 (2019) 861–877, https://doi.org/10.1107/S2059798319011471.
[30] P. Emsley, B. Lohkamp, W.G. Scott, K. Cowtan, Features and development of Coot, Acta Crystallogr. D Biol. Crystallogr. 66 (2010) 486–501, https://doi.org/10.1107/S0907444910007493.
[31] G. Bricogne, E. Blanc, M. Brandl, C. Flensburg, P. Keller, W. Paciorek, P. Roversi, A. Sharff, O.S. Smart, C. Vonrhein, T.O. Womack, BUSTER Version 2.10.1, Global Phasing Ltd., Cambridge, United Kingdom, 2016.
[32] V.B. Chen, W.B. Arendall 3rd, J.J. Headd, D.A. Keedy, R.M. Immormino, G. J. Kapral, L.W. Murray, J.S. Richardson, D.C. Richardson, MolProbity: all-atom structure validation for macromolecular crystallography, Acta Crystallogr. D Biol. Crystallogr. 66 (2010) 12–21, https://doi.org/10.1107/S0907444909042073.
[33] E. Krissinel, K. Henrick, Inference of macromolecular assemblies from crystalline state, J. Mol. Biol. 372 (2007) 774–797, https://doi.org/10.1016/j.jmb.2007.05.022.
[34] B. Kozlikova, E. Sebestova, V. Sustr, J. Brezovsky, O. Strnad, L. Daniel, D. Bednar, A. Pavelka, M. Manak, M. Bezdeka, P. Benes, M. Kotry, A. Gora, J. Damborsky, J. Sochor, CAVER Analyst 1.0: graphic tool for interactive visualization and analysis of tunnels and channels in protein structures, Bioinformatics 30 (2014) 2684–2685, https://doi.org/10.1093/bioinformatics/btu364.
[35] O.N. Lemaire, P. Infossi, A. Ali Chaouche, L. Espinosa, S. Leimkühler, M.-T. Giudici-Orticoni, V. Méjean, C. Iobbi-Nivol, Small membranous proteins of the TorE/NapE family, crutches for cognate respiratory systems in *Proteobacteria*, Sci. Rep. 8 (2018) 13576, https://doi.org/10.1038/s41598-018-31851-2.
[36] Y. Kung, T.I. Doukov, J. Seravalli, S.W. Ragsdale, C.L. Drennan, Crystallographic snapshots of cyanide- and water-bound C-clusters from bifunctional carbon monoxide dehydrogenase/acetyl-CoA synthase, Biochemistry 48 (2009) 7432–7440, https://doi.org/10.1021/bi900574h.
[37] T.I. Doukov, T.M. Iverson, J. Seravalli, S.W. Ragsdale, C.L. Drennan, A Ni-Fe-Cu center in a bifunctional carbon monoxide dehydrogenase/acetyl-CoA synthase, Science 298 (2002) 567–572, https://doi.org/10.1126/science.1075843.
[38] S.W. Ragsdale, L.G. Ljungdahl, D.V. DerVartanian, Isolation of carbon monoxide dehydrogenase from *Acetobacterium woodii* and comparison of its properties with those of the *Clostridium thermoaceticum* enzyme, J. Bacteriol. 155 (1983) 1224–1237.
[39] J. Bertsch, V. Müller, CO metabolism in the Acetogen *Acetobacterium woodii*, Appl. Environ. Microbiol. 81 (2015) 5949, https://doi.org/10.1128/AEM.01772-15.
[40] L. Domnik, M. Merrouch, S. Goetzl, J.-H. Jeoung, C. Léger, S. Dementin, V. Fourmond, H. Dobbek, CODH-IV: a high-efficiency CO-scavenging CO dehydrogenase with resistance to O_2, Angew. Chem. Int. Ed. 56 (2017) 15466–15469, https://doi.org/10.1002/anie.201709261.
[41] J. Fesseler, J.-H. Jeoung, H. Dobbek, How the $[NiFe_4S_4]$ cluster of CO dehydrogenase activates CO_2 and NCO−, Angew. Chem. Int. Ed. 54 (2015) 8560–8564, https://doi.org/10.1002/anie.201501778.
[42] E.C. Wittenborn, M. Merrouch, C. Ueda, L. Fradale, C. Leger, V. Fourmond, M. E. Pandelia, S. Dementin, C.L. Drennan, Redox-dependent Rearrangements of the NiFeS Cluster of Carbon Monoxide Dehydrogenase, Elife 7, 2018, https://doi.org/10.7554/eLife.39451.
[43] C.L. Drennan, J. Heo, M.D. Sintchak, E. Schreiter, P.W. Ludden, Life on carbon monoxide: X-ray structure of *Rhodospirillum rubrum* Ni-Fe-S carbon monoxide dehydrogenase, Proc. Natl. Acad. Sci. 98 (2001) 11973–11978, https://doi.org/10.1073/pnas.211429998.
[44] H. Dobbek, V. Svetlitchnyi, J. Liss, O. Meyer, Carbon monoxide induced decomposition of the active site [Ni−4Fe−5S] cluster of CO dehydrogenase, J. Am. Chem. Soc. 126 (2004) 5382–5387, https://doi.org/10.1021/ja037776v.
[45] S.W. Ragsdale, H.G. Wood, Acetate biosynthesis by acetogenic bacteria. Evidence that carbon monoxide dehydrogenase is the condensing enzyme that catalyzes the final steps of the synthesis, J. Biol. Chem. 260 (1985) 3970–3977.
[46] S.I. Hu, H.L. Drake, H.G. Wood, Synthesis of acetyl coenzyme A from carbon monoxide, methyltetrahydrofolate, and coenzyme A by enzymes from *Clostridium thermoaceticum*, J. Bacteriol. 149 (1982) 440–448.
[47] W.F. Martin, R.K. Thauer, Energy in ancient metabolism, Cell 168 (2017) 953–955, https://doi.org/10.1016/j.cell.2017.02.032.
[48] E. Kocsis, M. Kessel, E. DeMoll, D.A. Grahame, Structure of the Ni/Fe-S protein subcomponent of the acetyl-CoA decarbonylase/synthase complex from *Methanosarcina thermophila* at 26-Å resolution, J. Struct. Biol. 128 (1999) 165–174, https://doi.org/10.1006/jsbi.1999.4163.
[49] C. Darnault, A. Volbeda, E.J. Kim, P. Legrand, X. Vernede, P.A. Lindahl, J. C. Fontecilla-Camps, Ni-Zn-$[Fe_4$-$S_4]$ and Ni-Ni-$[Fe_4$-$S_4]$ clusters in closed and open subunits of acetyl-CoA synthase/carbon monoxide dehydrogenase, Nat. Struct. Biol. 10 (2003) 271–279, https://doi.org/10.1038/nsb912.
[50] X. Tan, H.K. Loke, S. Fitch, P.A. Lindahl, The tunnel of acetyl-coenzyme A synthase/carbon monoxide dehydrogenase regulates delivery of CO to the active site, J. Am. Chem. Soc. 127 (2005) 5833–5839, https://doi.org/10.1021/ja043701v.
[51] V. Svetlitchnyi, H. Dobbek, W. Meyer-Klaucke, T. Meins, B. Thiele, P. Römer, R. Huber, O. Meyer, A functional Ni-Ni-[4Fe-4S] cluster in the monomeric acetyl-CoA synthase from *Carboxydothermus hydrogenoformans*, Proc. Natl. Acad. Sci. U. S. A. 101 (2004) 446–451, https://doi.org/10.1073/pnas.0304262101.

[52] W. Buckel, R.K. Thauer, Flavin-based electron bifurcation, a new mechanism of biological energy coupling, Chem. Rev. 118 (2018) 3862–3886, https://doi.org/10.1021/acs.chemrev.7b00707.
[53] P.-L. Tremblay, T. Zhang, S.A. Dar, C. Leang, D.R. Lovley, The Rnf complex of *Clostridium ljungdahlii* is a proton-translocating ferredoxin: NAD^+ oxidoreductase essential for autotrophic growth, mBio 4 (2012) e00406-e00412, https://doi.org/10.1128/mBio.00406-12.
[54] S. Wang, H. Huang, J. Moll, R.K. Thauer, $NADP^+$ reduction with reduced ferredoxin and $NADP^+$ reduction with NADH are coupled via an electron-bifurcating enzyme complex in *Clostridium kluyveri*, J. Bacteriol. 192 (2010) 5115–5123, https://doi.org/10.1128/JB.00612-10.
[55] P.S. Adam, G. Borrel, S. Gribaldo, Evolutionary history of carbon monoxide dehydrogenase/acetyl-CoA synthase, one of the oldest enzymatic complexes, Proc. Natl. Acad. Sci. U. S. A. 115 (2018) E1166–E1173, https://doi.org/10.1073/pnas.1716667115.
[56] S.M. Techtmann, A.V. Lebedinsky, A.S. Colman, T.G. Sokolova, T. Woyke, L. Goodwin, F.T. Robb, Evidence for horizontal gene transfer of anaerobic carbon monoxide dehydrogenases, Front. Microbiol. 3 (2012) 132, https://doi.org/10.3389/fmicb.2012.00132.
[57] M. Inoue, I. Nakamoto, K. Omae, T. Oguro, H. Ogata, T. Yoshida, Y. Sako, Structural and phylogenetic diversity of anaerobic carbon-monoxide dehydrogenases, Front. Microbiol. 9 (2019) 3353, https://doi.org/10.3389/fmicb.2018.03353.
[58] W. Gong, B. Hao, Z. Wei, D.J. Ferguson Jr., T. Tallant, J.A. Krzycki, M.K. Chan, Structure of the $\alpha_2\varepsilon_2$ Ni-dependent CO dehydrogenase component of the *Methanosarcina barkeri* acetyl-CoA decarbonylase/synthase complex, Proc. Natl. Acad. Sci. U. S. A. 105 (2008) 9558–9563, https://doi.org/10.1073/pnas.0800415105.